Journal of ELECTRONIC MATERIALS, Vol. 49, No. 5, 2020
https://doi.org/10.1007/s11664-020-08051-8


# Dielectric and Magnetic Properties of Polyaniline-Blended Y-Type $Ba_2Ni_2Fe_{12}O_{22}$ Hexaferrite Composites

G. PACKIARAJ,[1] K. SAKTHIPANDI,[2,5] RAJSHREE B. JOTANIA,[3] and ASLAM HOSSAIN[4]

1.—Department of Physics, Aditya College of Engineering, Surampalem, Andhra Pradesh 533 437, India. 2.—Department of Physics, Sethu Institute of Technology, Kariapatti, Tamil Nadu 626 115, India. 3.—Department of Physics, Electronics and Space Science, University School of Sciences, Gujarat University, Ahmedabad, Gujarat 380 009, India. 4.—Department of Physical and Inorganic Chemistry, Institute of Natural Sciences and Mathematics, Ural Federal University, Yekaterinburg, Russia. 5.—e-mail: sakthipandi@gmail.com

Polyaniline was blended to tune the magnetic properties of $Ba_2Ni_2Fe_{12}O_{22}$ hexaferrites. Polyaniline-blended $Ba_2Ni_2Fe_{12}O_{22}$ hexaferrite (weight ratios 1:1, 1:2 and 2:1) composites were prepared by the in situ polymerization method. The obtained polymer-blended ferrite composites were characterized by Fourier transform infrared spectroscopy, x-ray diffraction (XRD), scanning electron microscopy, and vibrating-sample magnetometer and low-frequency (20 Hz–2 MHz) dielectric measurements at room temperature. The presence of the hexagonal phases was detected in XRD peaks of $Ba_2Ni_2Fe_{12}O_{22}$ and polymer-blended hexaferrite composites. The dielectric studies showed that polyaniline-embedded hexaferrites have high values of dielectric constants compared with Y-type $Ba_2Ni_2Fe_{12}O_{22}$ hexaferrite. In addition, the saturation magnetization, coercivity and remanence magnetization of undoped $Ba_2Ni_2Fe_{12}O_{22}$ hexaferrite were decreased and tuned with the polyaniline concentration (from 43.98 emu/g to 9.32 emu/g, 611 Oe to 125 Oe, and 22.4 emu/g to 2.7 emu/g, respectively). Thus, the prepared polymer-blended hexaferrite composites showed promising magnetic and dielectric properties.

**Key words:** PANI, polymer-ferrite composite, hard ferrite, structural properties, magnetic properties

## INTRODUCTION

Over the past few years, there have been enormous developments in the field of science and technology, particularly in electronics.[1–3] The development of ferrite composites plays an essential role in reducing electromagnetic interference.[4] The recent research on Y-type hexagonal ferrites has studied different applications due to their very low dielectric loss, high uniaxial anisotropy, high magnetization and good chemical stability.[5,6] These hexaferrites contain a major component of ferric oxide ($Fe_2O_3$) in combination with divalent oxides such as BaO, SrO or PbO. Other conventional magnetic materials cannot replace ferrites because ferrites are stable, relatively inexpensive and have a wide range of industrial applications in operating devices, transformer cores, high- and very-high-frequency circuits, and high-quality filters.[7] The interesting magnetic properties of Y-type hexaferrites have been detected in hyper-frequency. Y-type hexagonal ferrites established in a hyper-frequency range can meet all the necessary criteria of conventional soft magnetic materials for chip component-type hexaferrites with planar magnetic anisotropy having higher cutoff frequency than spinel ferrites.[8,9]

Numerous structural ferrites have garnered the attention of material science researchers over the years. Crystal structures and properties have been

(Received October 12, 2019; accepted February 26, 2020; published online March 10, 2020)

reported for several hexaferrite-type materials, including M-type ($Me_2Fe_{12}O_{19}$; Me denotes the first transition divalent cations), X-type ($Ba_2Me_2Fe_{28}O_{46}$), W-type ($BaMe_2Fe_{16}O_{27}$), Y-type ($BaMe_2Fe_{12}O_{22}$), U-type ($Ba_4Me_2Fe_{36}O_{60}$) and Z-type ($Ba_3Me_2Fe_{24}O_{41}$).[10–13] Different techniques including hydrothermal, combustion, coprecipitation and oxidation, sol–gel, solid-state, flux, spray pyrolysis and evaporative decomposition of misted solutions have been used for the preparation of hexaferrite powder.[14–16] The physicochemical properties of hexaferrite are influenced by preparation conditions, chemical composition, amount of substitutions, sintering temperature and time. Numerous features concerning the microstructure, magnetic properties, phase formation process and thermal characterization of Y-type hexaferrites have been investigated in the literature.[6,17,18] Y-type $Ba_2Ni_2Fe_{12}O_{22}$ (BNFO) hexaferrite with a complex crystal structure has been less studied.

Hexaferrite materials with narrow particle size distribution may be promising for engineering applications.[19] In a recent work, Mohsen et al. successfully prepared $BaM/Fe_3O_4$ (hard/soft) nanocomposites in order to enhance $(BH)_{max}$, and a 75% increase in $(BH)_{max}$ was observed in $BaM/Fe_3O_4$ nanocomposites, with a 9:1 weight ratio.[20] Polycrystalline hexaferrites are very useful because of their ability to absorb electromagnetic radiation.[21] However, the absorption properties of hexaferrites can be tuned to obtain the desired electromagnetic characteristics by blending a polymer with them. Blending of a polymer with hexaferrites represents a dominant approach to tune the characteristics of the ferrites. The features of these polymers make them suitable for use in a wide range of applications in electroluminescent devices, integrated waveguides, color displays, microwave devices and polymeric optical fibers.[22–24] A team of researchers from the Indian Institute of Sciences, Bangalore, India, studied the various aspects and characteristics of electromagnetic shielding using different Ba-Pb-hexaferrite,[25] yttrium iron garnet-polyaniline-wax composites,[26] Ba-Pb-hexaferrite-polyaniline-wax nanocomposites,[27] and lead hexaferrite/polyaniline composite.[28]

Polyaniline (PANI) is a conducting polymer whose transport, optical and magnetic properties are dependent on the extent that it has been doped by charge transfer of the materials, and demonstrates great potential due to its stretched *p*-conjugated skeletons and higher absorption efficiency in the visible-light range.[29,30] Non-redox doping of PANI leads to a polaron lattice with acceptable thermal stability and electrical conductivity.[31] In addition, PANI is one of the extensively investigated polymers due to its low cost, air stability, apparent chemistry and metallurgical behavior.[32] The aim of this work is to investigate the structural, dielectric and magnetic properties of $Ba_2Ni_2Fe_{12}O_{22}$ composites based on blended polyaniline. For this, polyaniline (PANI)/BNFO composites were prepared with different weight ratios (1:1, 1:2 and 2:1) using an in situ polymerization technique. As-prepared composite materials were characterized using x-ray diffraction (XRD), Fourier transform infrared (FTIR) spectroscopy, scanning electron microscopy (SEM), vibrating-sample magnetometer (VSM) and low-frequency dielectric measurements at room temperature.

## EXPERIMENTAL PROCEDURE

### Synthesis of Polyaniline/$Ba_2Ni_2Fe_{12}O_{22}$ Composites

Aniline ($C_6H_5NH_2$; Merck, GR grade), ammonium persulfate [$(NH_4)_2S_2O_8$; Merck, GR grade], 0.1 M HCl solution and Y-type BNFO hexaferrite were taken as raw materials to prepare a polyaniline-blended BNFO composites. A sol–gel auto-combustion method was used to synthesize Y-type BNFO hexaferrites.[33] The obtained combusted powder was heated at 500°C for 4 h and then finally calcined at 950°C for 4 h to prepare the Y-type BNFO hexaferrite powder. In this preparation method, a certain quantity of ferrite powder was suspended in 0.1 M HCl, and the mixture was vigorously stirred at room temperature for 1 h to obtain a fine aqueous dispersion. Aniline monomer was then added to the prepared mixture, and composite ratios of aniline to hexaferrite powder were taken at 1:2, 1:1 and 2:1 weight proportions. The monomer-ferrite dispersion was stirred for 2 h and then cooled to 5°C. A stoichiometric amount of ammonium persulfate (molar ratio aniline: $(NH_4)_2S_2O_8$ at 1:1) was dissolved in 0.1 M HCl and then slowly added dropwise into the suspension mixture under constant stirring. The polymerization was allowed to proceed for $\sim$ 10 h at 5°C, after which a dark green solution was recovered. Finally, the solution was filtered and washed repeatedly with 0.1 M HCl and deionized distilled water to obtain the composites. The wet polyaniline-coated particles were then dried at 60°C for 24 h. The processing flow chart for preparing the polyaniline-blended BNFO composites is shown in Fig. 1. As-prepared samples were coded as BNFO12, BNFO11 and BNFO21 for aniline to $Ba_2Ni_2Fe_{12}O_{22}$ hexaferrite in a weight ratio of 1:2, 1:1 and 2:1, respectively.

### Characterization of Polyaniline-Blended $Ba_2Ni_2Fe_{12}O_{22}$ Composites

The x-ray diffraction (XRD) patterns of BNFO hexaferrite and polyaniline-blended BNFO composite samples were recorded at room temperature using a Seifert XRD 3000 PTS diffractometer equipped with a $CuK_\alpha$ ($\lambda$ = 1.5405 Å) radiation source. The XRD spectra were recorded at a diffraction angle ($2\theta$) from 20° to 80° at a rate of 2°/min. The Fourier transform infrared (FTIR) spectra of BNFO hexaferrite and polyaniline-blended BNFO

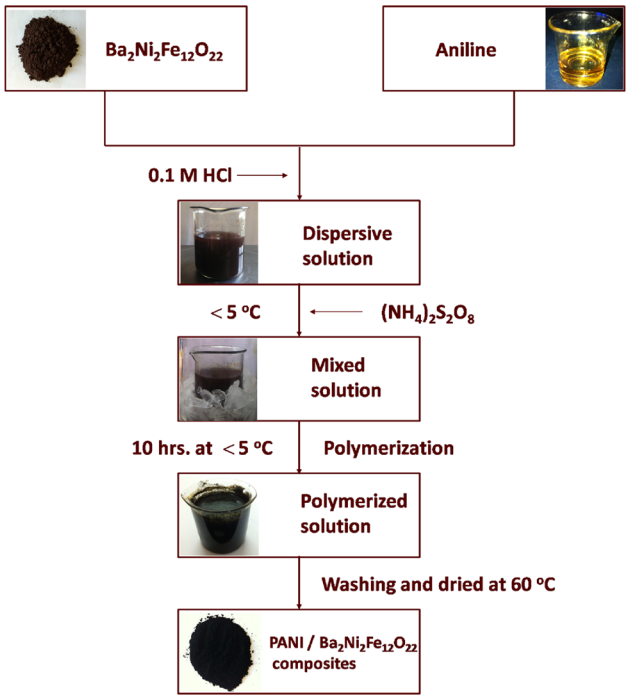


Fig. 1. Schematic representation of the preparation of polyaniline/$Ba_2Ni_2Fe_{12}O_{22}$ composites.

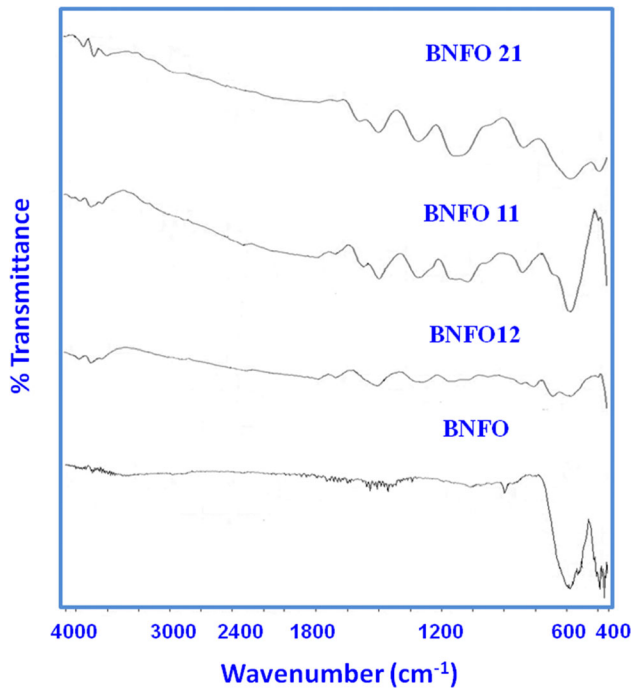


Fig. 2. FTIR spectra of BNFO, BNFO12, BNFO11 and BNFO21 samples.

composite samples were recorded at room temperature in the wavenumber range of 4000 $cm^{-1}$ to 400 $cm^{-1}$ using an FTIR Bruker Tensor 27 spectrometer. The surface morphology of BNFO hexaferrite and polyaniline-blended BNFO composite samples was examined with a scanning electron microscope (SEM; LEO 440i) equipped with a NORAN x-ray microanalysis system. These composites are highly resistive materials, so they do not provide a path to ground for the specimen current ($I_s$) and may undergo electrostatic charging when exposed to the electron probe. To prevent the charging problem, each sample was coated with a thin layer of gold using an ion -sputter coater. Field-dependent magnetization measurements of BNFO hexaferrite and polyaniline-blended BNFO composite materials were carried out at room temperature using a VSM (EG&G Princeton Applied Research; Model 4500). Approximately 10 mg powder sample was tightly filled in a small nonmagnetic plastic tube and mounted on the VSM sample holder. The hysteresis curve was then recorded under an applied magnetic field of ± 15 KOe. The dielectric measurement was taken at room temperature using an Agilent E-4980A precision inductance, capacitance and resistance meter. Simultaneous measurements of capacitance ($C_p$) and equivalent parallel resistance ($R_p$) were recorded for a frequency range of 20 Hz–5 MHz. Circular pellets of 13 mm diameter and ~ 2 mm thickness were prepared for dielectric measurement. The pellet faces were coated with a silver paste to make good contact with electrodes.

## RESULTS AND DISCUSSION

Figure 2 shows the FTIR spectra of Y-type BNFO hexaferrite and polyaniline-blended BNFO hexaferrite samples. Two strong and sharp absorption bands were found for BNFO hexaferrite near 580 $cm^{-1}$ and 440 $cm^{-1}$, which are characteristic infrared absorption bands due to the presence of stretching vibrations of the metal–oxygen bond.[34] The characteristic peaks of polyaniline appear at 1587 $cm^{-1}$, 1496 $cm^{-1}$, 1303 $cm^{-1}$, 1130 $cm^{-1}$ and 802 $cm^{-1}$ for BNFO12, BNFO11 and BNFO21 composite samples.[35,36] The peaks at 1587 $cm^{-1}$ and 1496 $cm^{-1}$ are attributed to the characteristic C=C stretching of the quinoid and benzenoid rings, respectively; the peak at 1303 $cm^{-1}$ is assigned to C–N stretching of the benzenoid ring; and the broad and strong peak around 1130 $cm^{-1}$ is associated with the vibration modes of N=Q=N (Q refers to the quinonic-type rings). The peak at 802 $cm^{-1}$ corresponds to the out-of-plane deformation vibration of the *p*-disubstituted benzene ring. FTIR spectra of BNFO12, BNFO11 and BNFO21 composites confirmed that an increase in the polyaniline content in hexaferrite specifically leads to intensity band characteristics corresponding to polyaniline. The FTIR spectrum of PANI is available in existing literature.[30,37] The peaks observed at 1573 (for the quinoid ring) and 1489 $cm^{-1}$ (for benzenoid ring) are attributed to the C=C stretching. Tilting of the N–H bending (at 1298 $cm^{-1}$) and C–H asymmetric broadening modes of the benzenoid ring (1247 $cm^{-1}$) were observed. In addition, fluctuations in the transmittance FTIR spectrum around 1300 $cm^{-1}$

were observed due to the existence of trapped nitrates in the BNFO sample.[38] Liu and Zhu[30] revealed that the strong band presented (vibration mode of N=Q=N) at 1116 $cm^{-1}$ corresponds to the doped PANI with graphene oxide/$Fe_3O_4$. The observed band at 1130 $cm^{-1}$ is used to confirm the doping of the hexaferrites with PANI.

The XRD patterns of BNFO hexaferrite and polyaniline-blended BNFO composite samples are shown in Fig. 3. XRD peaks were indexed using Powder-X software, and obtained reflection peaks were compared with standard JCPDS card no. 82-0472 of $Ba_2Co_2Fe_{12}O_{22}$ ($a$ = 8596 Å, $c$ = 43.502 Å, rhombohedral). XRD analysis of BNFO sample shows formation of the pure phase. The lattice parameters were found as $a$ = 5.839 Å and $c$ = 43.386 Å. There are no intermediate phases such as $\alpha$-$Fe_2O_3$, $\gamma$-$Fe_2O_3$, $BaCO_3$, $BaFe_2O_4$ and $NiFe_2O_4$. The XRD patterns of polyaniline-blended BNFO composites show the characteristic peaks of both BNFO and polyaniline (JCPDS card no. 53-1891). Polyaniline is semicrystalline with a certain degree of crystallinity. The comparative intensity of the peaks corresponding to different composites might differ due to the amount of aniline and BNFO ferrite compositions. It is interesting to note that the crystalline peaks corresponding to polyaniline-blended BNFO composite samples are similar to those of BNFO ferrite.[39,40]

The lattice constants and crystallite size of BNFO hexaferrite and polyaniline-blended BNFO composite samples were obtained from XRD patterns using standard formulae.[41–43] The crystalline size can be estimated using the simple Scherrer's formula by measuring the inter-planar spacing (d-spacing) for reflections viewed from 2$\theta$ values, which represent the distance between the planes of the benzene ring of two adjacent chains. The obtained values are given in Table I. It is inferred that the crystallite size of BNFO hexaferrite further decreases due to blending of polyaniline with materials. Polyaniline was used to inhibit the growth of the grains. Thus, crystallite size decreased with an increase in the polyaniline concentration. The observed results for BNFO hexaferrite and polyaniline-blended BNFO composite samples are similar to those observed in some earlier studies on ferrites.[44–46] Very recently, Choudhary et al.,[27] Kagotani et al.[47] and Feng et al.[48] reported the XRD pattern of PANI. The XRD pattern consists of two typical peaks at 2$\theta$ = 20.4° and 26.28° for Choudhary et al.[27], and one characteristics peak at ~ 25.41° for Feng et al.[48], showing the semicrystalline nature of PANI. $PANI_x/Bi_2MoO_6$ nanocomposites were prepared and studied.[48] Similar XRD patterns between the $PANI_x/Bi_2MoO_6$ nanocomposites and the pure $Bi_2MoO_6$ reveal that PANI with lower content shows no significant adverse impact on the crystallinity of $Bi_2MoO_6$. However, the higher ratio of the PANI content with the nanocomposite may change the crystalline nature of the nanocomposites. Therefore, the concentration in unit cells was investigated in the composite with higher PANI content.

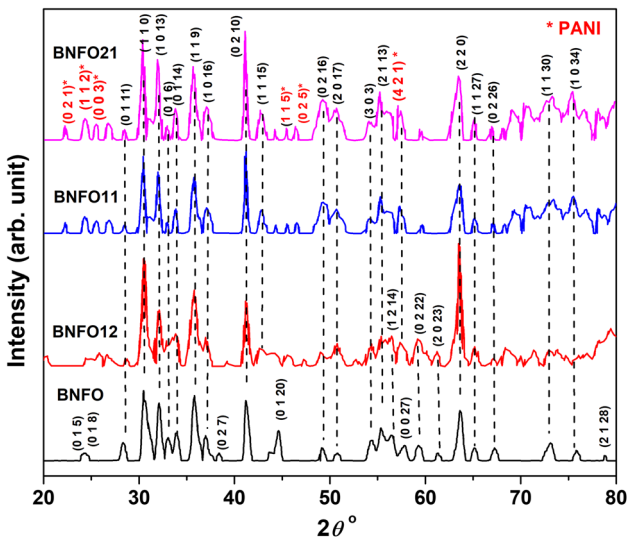


Fig. 3. XRD patterns of BNFO, BNFO12, BNFO11 and BNFO21 samples.

Figure 4 shows SEM images of Y-type BNFO hexaferrite and polyaniline-blended BNFO hexaferrite samples. The SEM of Y-type BNFO hexaferrite shows a hexagonal plate-like structure. Different structures were observed when hexaferrite was blended with a polyaniline. The SEM images of BNFO11, BNFO12 and BNFO21 composites show that polyaniline was deposited on the surface of ferrite particles, which have coral-like structure. In general, polymers were used to tune the particle size of oxides.[49] In line with the XRD crystallite size of the BNFO and doped BNFO samples, the particle size decreases with an increase in the concentration of PANI in the composite. In addition, it is evident from SEM that the morphology of the BNFO sample (e.g., hexagonal to coral) was changed by adding PANI.

The variation of the dielectric constant (real-$\varepsilon'$) as a function of frequency for Y-type BNFO hexaferrite and polyaniline-blended BNFO samples is shown in Fig. 5. It can be observed that the dielectric constant (real) of Y-type BNFO hexaferrite and polyaniline-blended BNFO hexaferrite samples decreases with the increase in frequency. The dielectric nature of Y-type BNFO hexaferrite is determined based on the Verwey mechanism and Heiks model.[50] In the case of BNFO12, BNFO11 and BNFO21 composites, there were two types of charged species: one is the polaron/bipolaron system, which is transportable and allows transfer along the chain, and the others are bound charges (dipoles), which have restricted transfer and account for strong polarization in the hexaferrite.[51]

The BNFO12 and BNFO11 ferrite-PANI composites show a higher value than the pure BNFO and BNFO21 composites, which reveals that the dielectric loss increases in BNFO12 and BNFO11 ferrite-

**Table I. Lattice parameters and crystallite size of BNFO, BNFO12, BNFO11 and BNFO21 samples**

| Sample | Lattice constant | | Unit cell volume (Å$^3$) | Crystallite size (nm) |
|---|---|---|---|---|
| | *a* (Å) | *c* (Å) | | |
| BNFO | 5.839 | 43.386 | 1280.986 | 48.986 |
| BNFO12 | 5.854 | 43.388 | 1287.636 | 42.157 |
| BNFO11 | 5.866 | 43.396 | 1293.158 | 37.972 |
| BNFO21 | 5.827 | 43.383 | 1275.638 | 31.663 |

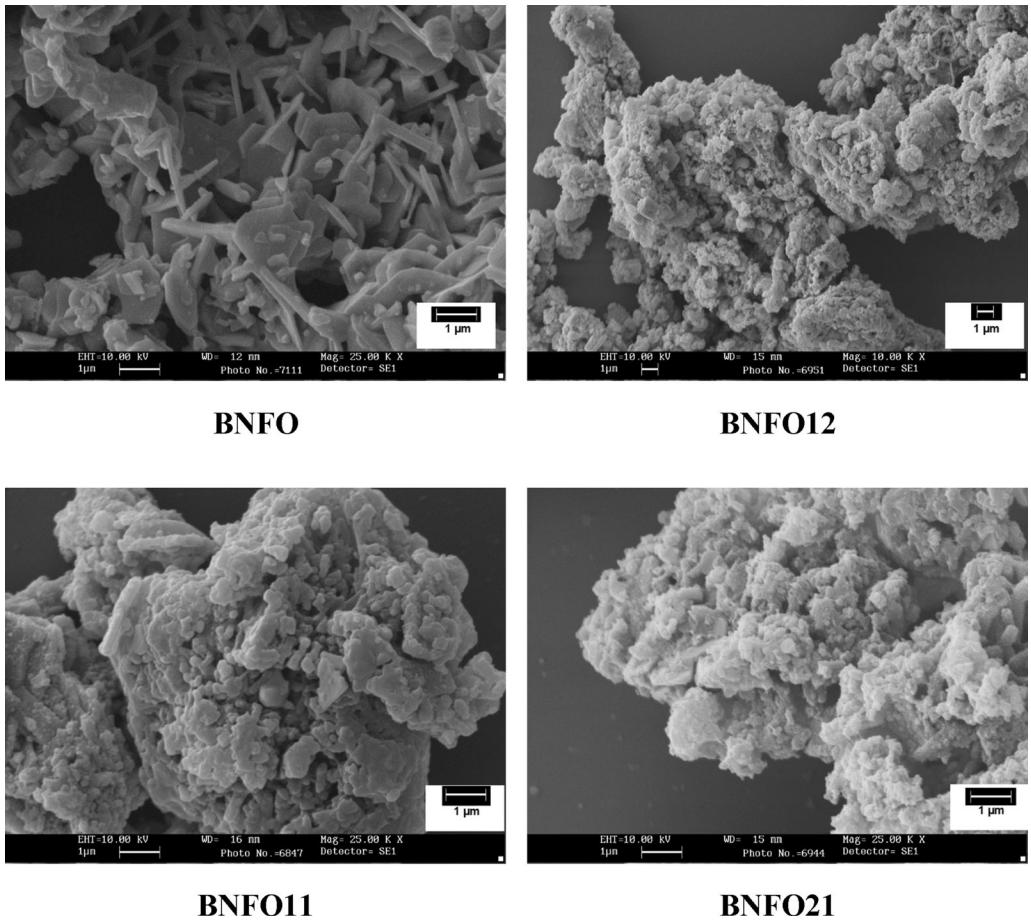


Fig. 4. SEM images of BNFO, BNFO12, BNFO11 and BNFO21 samples.

PANI composites. The integration of polyaniline in the BNFO ferrite composite improves the AC conductivity. This is primarily due to the establishment of the micro-capacitors through the ferrite particles sandwiched between the polyaniline. It is worth noting that PANI has a conducting nature, and hexaferrites are electrical insulators. Hence, the capacitive behavior of the ferrite-PANI composites was created through the electron hopping in PANI, resulting in the loss in conduction of the composites. However, the further increase in PANI concentration with BNFO leads to a decrease in the dielectric nature. Therefore, an optimum balance between the concentration of ferrites and PANI is important in achieving improved electromagnetic shielding.[27]

In the ferrite PANI composite, ferrite particles act as a dielectric medium between the PANI chains and produce nano-capacitors in the composites. To attain desirable electrical conductivity of the nanocomposites, the conducting polymer, PANI, was dispersed as a conductive phase. The incorporation of polyaniline in Y-type BNFO hexaferrite composite enhances the AC conductivity. This is mainly due to the creation of the micro-capacitors through the hexaferrite particles sandwiched between the polyaniline fibers. This leads to the capacitive behavior of the hexaferrite and electron

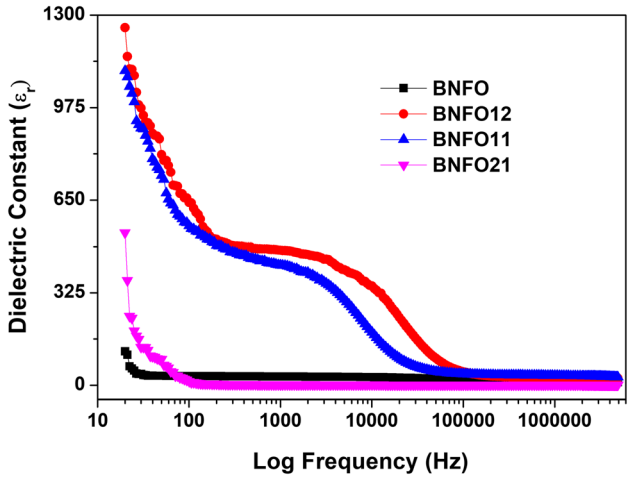


Fig. 5. Variation of dielectric constant ($\varepsilon'$) as a function of frequency for BNFO, BNFO12, BNFO11 and BNFO21 samples.

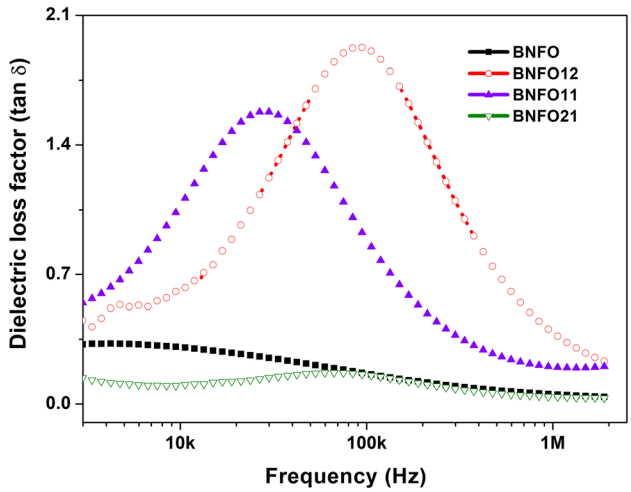


Fig. 6. Variation of dielectric loss tangent (tan $\delta$) as a function of frequency for BNFO, BNFO12, BNFO11 and BNFO21 samples.

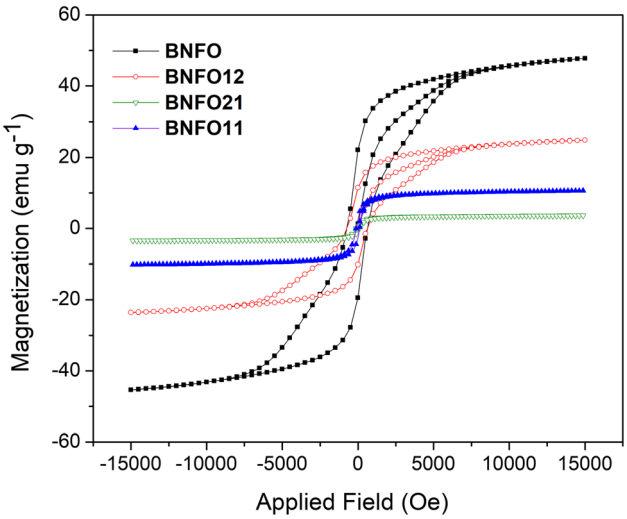


Fig. 7. M–H curves of BNFO, BNFO12, BNFO11 and BNFO21 samples.

hopping in PANI, resulting in the conduction loss in the composite. This behavior is attributable to BNFO ferrite particles that are embedded in the PANI matrix, as the interaction between the polymer matrix and ferrite particles increases the charge carrier scattering and thus increases the dielectric constant of the BNFO12 and BNFO11 ferrite sample. However, the interaction was broken by the excess polymer concentration, and hence the dielectric constant was decreased for the BNFO21 ferrite sample. When a signal with high frequency enters through these nano-capacitors, a phase lag builds dielectric relaxation. Hence, microwave absorption in the composites was achieved through these dielectric relaxations.[27,31]

The combined effect of the relaxation of magnetic dipoles and magnetic loss due to ferromagnetic resonance presented in the magnetic nanoparticles and the relaxation of electric dipoles and electrical conduction present in the PANI are the main cause of the shielding of microwave radiation in the nanocomposite. Thus, the incorporation of PANI led to an improved shielding efficiency of the PANI-BNFO composite. The interfaces in the PANI-BNFO composite were controlled by the Maxwell–Wagner polarization. This caused a huge dielectric relaxation which gave rise to the microwave absorption properties.

The gradual increase in the frequency of the applied field was unable to achieve the desired reorientation of hexaferrites dipoles, resulting in a decrease in the dielectric constant. BNFO12 and BNFO11 composites showed high values of dielectric constants compared with the BNFO hexaferrite sample. Initially, for composites with aniline-to-hexaferrite weight ratios of 1:2 and 1:1, the dielectric constant reaches the highest value with a little amount of polyaniline (BNFO12) and then decreases with increase in polyaniline in the composite (BNFO11). However, the dielectric constant of BNFO21 is similar to that of Y-type BNFO hexaferrite. Thus, the dielectric properties were tuned with the blending concentration of polyaniline.[52,53] The variation of dielectric loss tangent (tan$\delta$) as a function of the frequency of Y-type BNFO hexaferrite and polyaniline-blended BNFO hexaferrite samples is shown in Fig. 6. It is interesting to note that there is no variation in the dielectric loss tangent of Y-type BNFO and BNFO21 over a wide frequency range. However, a peak in tan$\delta$ is observed at a particular frequency for BNFO12 and BNFO11. The existence of peaks in the variation of dielectric loss tangent (Fig. 6) with frequency was detected when the frequency of hopping was nearly equal to that of the externally applied electric field, which suggests that the dielectric loss increases in the hexaferrite-PANI composites when the samples are sintered at 950°C. This observation is exactly the same as that with Ba-Pb-hexaferrites and PANI-doped Ba-Pb-hexaferrites.[47]

**Table II. Magnetic parameters of BNFO, BNFO12, BNFO11 and BNFO21 samples**

| Sample | Magnetization ($M_s$) (emu/g) | Coercivity ($H_c$) (Oe) | Retentivity ($M_r$) (emu/g) | Squareness ratio ($M_r/M_s$) (no. units) | Reference |
|---|---|---|---|---|---|
| BNFO | 43.98 | 611 | 22.4 | 0.509 | Current work |
| BNFO11 | 23.11 | 621 | 11.46 | 0.495 | Current work |
| BNF012 | 3.04 | 125 | 1.62 | 0.530 | Current work |
| BNFO21 | 9.32 | 125 | 2.7 | 0.289 | Current work |
| $Sr_2Cu_2Fe_{12}O_{22}$ | 60.1 | – | 27.5 | 0.457 | 59 |
| $Sr_2Cu_{0.2}Co_{0.8}Fe_{12}O_{22}$ | 18.03 | – | 8.9 | 0.486 | 59 |
| $Ba_2Co_2Fe_{12}O_{22}$ | 21.9 | 48.2 | 4.73 | 0.215 | 60 |
| $Ba_2Zn_{1.2}Cu_{0.8}Fe_{12}O_{22}$ | 34.5 | 85.95 | 4.05 | 0.12 | 61 |
| $Ba_2Co_2Fe_{12}O_{22}$ | 44.54 | 1897.7 | 21.79 | 0.489 | 62 |
| $Sr_2Mg_2Fe_{12}O_{22}$ | 42.44 | 21.33 | 10.05 | 0.236 | 63 |
| PANI-coated $BaFe_{12}O_{19}$ | ~ 40 | 4842 | 28.7 | 0.7175 | 64 |

Figure 7 shows M–H curves recorded at room temperature for Y-type BNFO hexaferrite, BNFO12, BNFO11 and BNFO21 composites. The coercively ($H_c$), saturation ($M_s$) and remanence ($M_r$) magnetization were calculated from the observed hysteresis loop and are given in Table II. The decline in the values of magnetic parameters is observed for all the polyaniline-blended BNFO composite samples. It is clear that BNFO ferrite cores are responsible for the magnetic behavior of BNFO12, BNFO11 and BNFO21 composites. According to the equation $M_s = \varphi m_s$, $M_s$ is related to the volume fraction of the particles ($\varphi$) and the saturation moment of a single particle ($m_s$).[54,55] It can be claimed that $M_s$ of the BNFO12, BNFO11 and BNFO21 composites primarily depends on the volume fraction of the magnetic hexaferrite particles.

The nonmagnetic polyaniline coating layer may have impeded total magnetization and thus decreased the saturation magnetization.[56] Polyaniline was deposited on the surface of hexaferrite crystallite boundaries during the polymerization process and affected the ferrite surface defects, such as cracks and pores. Moreover, it might be that the surface spin pinning of magnetic moments at the hexaferrite nanoparticle support interface[57] caused a subsequent decrease in magnetic surface anisotropy. The polyaniline composites give lower values of coercivity than the Y-type BNFO hexaferrite.[58] Therefore, the magnetic properties of the Y-type BNFO hexaferrite can be modified/tuned with a blending of polyaniline.

## CONCLUSION

Polyaniline-blended $Ba_2Ni_2Fe_{12}O_{22}$ composites with different weight ratios (1:1, 1:2 and 2:1) of PANI/$Ba_2Ni_2Fe_{12}O_{22}$ were prepared using in situ polymerization method. The FTIR spectra of polyaniline-blended $Ba_2Ni_2Fe_{12}O_{22}$ composites showed absorption bands corresponding to both metal–oxygen stretching vibrations and stretching of the quinoid and benzenoid rings. The XRD patterns showed the characteristic peaks of both $Ba_2Ni_2Fe_{12}O_{22}$ hexaferrite and polyaniline. The SEM images of the composites revealed that polyaniline is deposited on the surface of hexaferrite particles, which possesses a core–shell structure. Polyaniline-embedded hexaferrites showed high values of dielectric constants compared with the Y-type $Ba_2Ni_2Fe_{12}O_{22}$ hexaferrite. The ferrite particles act as a dielectric medium between the polyaniline chains and produce nano-capacitors in the composites. The saturation magnetization, coercivity and remanence magnetization values of undoped $Ba_2Ni_2Fe_{12}O_{22}$ hexaferrite were decreased (from 43.98 emu/g to 9.32 emu/g, 611 Oe to 125 Oe, and 22.4 emu/g to 2.7 emu/g, respectively). These prepared Y-type BNFO hexaferrite and polyaniline-blended BNFO hexaferrite composites showed remarkable magnetic and dielectric properties.

## ACKNOWLEDGMENTS

R.B. Jotania and G. Packiaraj are grateful to UGC, New Delhi, India for DRS-SAP-Phase I [F.530/10/DRS/2010 (SAP-I)].

## REFERENCES

1. T. Jungwirth, J. Sinova, A. Manchon, X. Marti, J. Wunderlich, and C. Felser, *Nat. Phys.* 14, 200 (2018).
2. M.T. Gray, S. Emori, B.A. Gray, H. Jeon, O.M.J. van't Erve, B.T. Jonker, and S. Kim, *Phys. Rev. Appl.* 9, 064039 (2018).
3. Y. Wang, Y. Liu, C. Wu, Q. Liu, L. Gao, J. Li, and H. Zhang, *J. Supercond. Nov. Magn.* 31, 455 (2018).
4. M. Verma, A.P. Singh, P. Sambyal, B.P. Singh, S.K. Dhawan, and V. Choudhary, *Phys. Chem. Chem. Phys.* 17, 1610 (2015).
5. Y. Kitagawa, Y. Hiraoka, T. Honda, T. Ishikura, H. Nakamura, and T. Kimura, *Nat. Mater.* 9, 797 (2010).
6. R.C. Pullar, *Prog. Mater Sci.* 57, 1191 (2012).
7. G.V. Harris, *IEEE Trans. Magn.* 48, 1075 (2012).
8. H.-S. Cho and S.-S. Kim, *IEEE. Trans. Magn.* 35, 3151 (1999).
9. X. Batlle, X. Obradors, J.R. Carvajal, M. Pernet, M.V. Cabanas, and M. Vallet, *J. Appl. Phys.* 70, 1614 (1991).
10. M.A. Ahmed, N. Okasha, M. Oaf, and R.M. Kershi, *J. Magn. Magn. Mater.* 314, 128 (2007).

11. N. Chen, K. Yang, and M. Gu, *J. Alloys Compd.* 490, 609 (2010).
12. M. Sugimoto, *J. Am. Ceram. Soc.* 82, 269 (1999).
13. G. Albanese, M. Carbucicchio, and G. Asti, *Appl. Phys.* 11, 81 (1976).
14. R. Arulmurugan, B. Jeyadevan, G. Vaidyanathan, and S. Sendhilnathan, *J. Magn. Magn. Mater.* 288, 470 (2005).
15. C. Surig, K.A. Hempel, and D. Bonnenberg, *Appl. Phys. Lett.* 63, 2836 (1993).
16. C. Upadhyay, D. Mishra, H.C. Verma, S. Anand, and R.P. Das, *J. Magn. Magn. Mater.* 260, 188 (2003).
17. K. Oda and T. Inui, *J. J. Jpn. Soc. Powder Powder Metall.* 46, 88 (1999).
18. H. Nakajima, H. Kawase, K. Kurushima, A. Kotani, T. Kimura, and S. Mori, *Phys. Rev. B* 96, 024431 (2017).
19. M.M. Hessien, M.M. Rashad, and K. El-Barawy, *J. Magn. Magn. Mater.* 320, 336 (2008).
20. F. Mohseni, R.C. Pullar, J.M. Vieira, and J.S. Amaral, *J. Alloys Compd.* 806, 120 (2019).
21. M.P. Horvath, *J. Magn. Magn. Mater.* 215, 171 (2000).
22. Z.L. Wang, *Wiley Encyclopedia of Electrical and Electronics Engineering*, ed. J.G. Webster (New York: Wiley, 1999), pp. 11–25.
23. A.G. Fox, S.E. Miller, and M.T. Weiss, *Bell Syst. Tech. J.* 34, 5 (1955).
24. M.L. Kales, *J. Appl. Phys.* 24, 604 (1953).
25. H.K. Choudhary, R. Kumar, A.V. Anupama, and B. Sahoo, *Ceram. Int.* 44, 8877 (2018).
26. H.K. Choudhary, R. Kumar, S.P. Pawar, A.V. Anupama, S. Bose, and B. Sahoo, *Chem. Sel.* 3, 2120 (2018).
27. H.K. Choudhary, R. Kumar, S.P. Pawar, S. Bose, and B. Sahoo, *J. Electron. Mater.* 49, 1618 (2020).
28. H.K. Choudhary, S.P. Pawar, S. Bose, and, B. Sahoo, *AIP Conference Proceedings*, vol. 1953(1) (AIP Publishing, 2018), p. 120061.
29. S. Bhadra and D. Khastgir, *Polym. Test.* 27, 851 (2008).
30. R. Liu and A. Zhu, *Polym. Compos.* 40, E1111 (2019).
31. P. Saini, V. Choudhary, K.N. Sood, and S.K. Dhawan, *J. Appl. Polym. Sci.* 113, 3146 (2009).
32. D.T. Seshadri and N.V. Bhat, *J. Polym. Sci. Part B Polym. Phys.* 45, 1127 (2007).
33. G. Packiaraj, N.R. Panchal, and R.B. Jotania, *Invertis J. Sci. Technol.* 5, 71 (2012).
34. W. Yuping, *Development of Barium Hexaferrite Composite Materials for Microwave Absorption*. Ph.D. dissertation (National University of Singapore, 2006).
35. L. Li, J. Jiang, and F. Xu, *Eur. Polym. J.* 42, 2221 (2006).
36. C.L. Yuan, Y.S. Hong, and C.H. Lin, *J. Magn. Magn. Mater.* 323, 1851 (2011).
37. B. Butoi, A. Groza, P. Dinca, A. Balan, and V. Barna, *Polymers* 9, 732 (2017).
38. A.V. Zalesskii, A.A. Frolov, T.A. Khimich, and A.A. Bush, *Phys. Solid State* 45, 141 (2003).
39. L.A. Bashkirov, G.P. Dudchik, T.A. But'ko, L. Ya Kris'ko, L.I. Kunitskii, G.S. Petrov, A.A. Shershavina, T.A. Shichkova, and G. Ya Fedorova, *Inorg. Mater.* 37, 737 (2001).
40. S.M. Abbas, R. Chatterjee, A.K. Dixit, A.V.R. Kumar, and T.C. Goel, *J. Appl. Phys.* 101, 074105 (2007).
41. E.S. Alhwaitat, S.H. Mahmood, M. Al-Hussein, O.E. Mohsen, Y. Maswadeh, I. Bsoul, and A. Hammoudeh, *Ceram. Int.* 44, 779 (2018).
42. K. Sakthipandi and V. Rajendran, *Mater. Charact.* 77, 70 (2013).
43. M. Deepty, C. Srinivas, K.V. Babu, E.R. Kumar, S.S. Meena, C.L. Prajapat, N.K. Mohan, and D.L. Sastry, *J. Magn. Magn. Mater.* 466, 60 (2018).
44. J. Jiang, L. Li, and M. Zhu, *React. Funct. Polym.* 68, 57 (2008).
45. N.S. Kommareddi, M. Tata, V.T. John, G.L. McPherson, M.F. Herman, Y.S. Lee, C.J. O'Connor, J.A. Akkara, and D.L. Kaplan, *Chem. Mater.* 8, 801 (1996).
46. S.M. Abbas, A.K. Dixit, R. Chatterjee, and T.C. Goel, *J. Magn. Magn. Mater.* 309, 20 (2007).
47. T. Kagotani, D. Fujiwara, S. Sugimoto, K. Inomata, and M. Homma, *J. Magn. Magn. Mater.* 272, E1813 (2004).
48. T.-T. Feng, H. Yin, H. Jiang, X. Chai, X. Li, D. Li, W. Jing, X.-H. Liu, and B. Sun, *New J. Chem.* 43, 9606 (2019).
49. A. Taubert, D. Palms, Ö. Weiss, M.T. Piccini, and D.N. Batchelder, *Chem. Mater.* 14, 2594 (2002).
50. A.M. Abo El Ataa and S.M. Attiab, *J. Magn. Magn. Mater.* 257, 165 (2003).
51. S. Bhadra, N.K. Singha, and D. Khastgir, *Curr. Appl. Phys.* 9, 396 (2009).
52. K. Iwauchi, *Jpn. J. Appl. Phys.* 10, 1520 (1971).
53. Ö. Yavuz, M.K. Ram, M. Aldissi, P. Poddar, and S. Hariharan, *J. Mater. Chem.* 15, 810 (2005).
54. T.M. Kwon, P.L. Frattini, L.N. Sadani, and M.S. Jhon, *Colloids Surf. A* 80, 47 (1993).
55. Y. Wang, Y. Huang, Q. Wang, Q. He, and L. Chen, *Appl. Surf. Sci.* 259, 486 (2012).
56. L. Li, H. Liu, Y. Wang, J. Jiang, and F. Xu, *J. Colloid Interf. Sci.* 321, 265 (2008).
57. Q. Song and Z.J. Zhang, *J. Am. Chem. Soc.* 126, 6164 (2004).
58. T.G. Carreno, M.P. Morales, and C.J. Serna, *Mater. Lett.* 43, 97 (2000).
59. R.B. Jotania and S.H. Mahmood, eds., *Magnetic Oxides and Composites* (Millersville: Materials Research Forum LLC, 2018).
60. G.F.M. Pires Júnior, H.O. Rodrigues, J.S. Almeida, E.O. Sancho, J.C. Góes, M.M. Costa, J.C. Denardin, and A.S.B. Sombra, *J. Alloys Compd.* 493, 326 (2010).
61. Y. Bai, J. Zhou, Z. Gui, L. Li, and L. Qiao, *J. Appl. Phys.* 101, 083907 (2007).
62. C. Zhang, J. Shi, X. Yang, L. De, and X. Wang, *Mater. Chem. Phys.* 123, 551 (2010).
63. R. Tholkappiyan, K. Vishista, and F. Hamed, *Pramana* 88, 27 (2017).
64. H.K. Choudhary, S.P. Pawar, R. Kumar, A.V. Anupama, S. Bose, and B. Sahoo, *Chem. Select* 2, 830 (2017).